ELSEVIER

Journal of Nuclear Materials 255 (1998) 180–188

journal of nuclear materials

Radioluminescence in amorphous silica: temperature dependence and relaxation

D.W. Cooke [a,*], B.L. Bennett [a], E.H. Farnum [a], D.E. Thomas [a,1], A.M. Portis [b]

[a] *Materials Science and Technology Division, Los Alamos National Laboratory, Los Alamos, NM 87545, USA*
[b] *Department of Physics, University of California, Berkeley, CA 94720-7300, USA*

Received 8 August 1997; accepted 26 January 1998

Abstract

Radioluminescence measurements on preform and fiber amorphous silica specimens have been made in the temperature interval 6 to 300 K and wavelength regime 300 to 800 nm. A typical spectrum consists of peaks at ~550 (main band) and ~650 (secondary band) nm, which are associated with self-trapped excitons and nonbridging oxygen hole centers of the silica lattice, respectively. Radioluminescence from the main band decays with increasing temperature and becomes undetectable in the 130 to 170 K range, consistent with the decay of self-trapped holes. Assuming the decrease in radioluminescence with temperature to be due to quenching of self-trapped exciton *radiative* recombination, with a spread in quenching barrier energy, we derive an expression of the form $L(T) = L(0)/[1 + AT + BT^2 + CT^3]$, which yields an excellent fit to the experimental data. An observed time-dependent relaxation of radioluminescence is associated with the enhancement of *nonradiative* recombination. © 1998 Elsevier Science B.V. All rights reserved.

PACS: 78.60.−b; 78.66.Jg; 78.40.−q

1. Introduction

The application of fiber optic technology to sensors and communications has led in recent years to significant advances in the quality of presently available fibers [1]. One notable use of fiber optics is to transmit optical signals (~400–700 nm) from the relatively inaccessible plasma region of a fusion reactor to external diagnostic instrumentation [2]. Studies carried out at JET [3] (Joint European Torus) and TFTR [4] (Tokamak Fusion Test Reactor) have shown that fibers subjected to neutrons and γ irradiation suffer not only long-term radiation damage, manifested as enhanced optical absorption, but also emit radioluminescence (RL) and Cherenkov radiation during exposure. Each of these radiation-induced effects alters optical transmission, thereby complicating evaluation of diagnostic signals [5,6]. Consequently, they must be either sufficiently ameliorated or properly characterized if the fibers are to be useful. Because silica-based fibers are candidate materials for diagnostic use in the proposed International Thermonuclear Experimental Reactor (ITER) [7], which is presently being designed, it is important to address these issues in a timely manner.

It is the general consensus that fibers comprised of low-OH silica cores and F-doped silica cladding are the best available materials for use in the harsh radiation environments of fusion reactors [8]. Accordingly, we have investigated the temperature dependence and relaxation of RL from relevant silica specimens.

Tanimura et al. [9] investigated luminescence from amorphous silica (a-SiO_2) following electron-pulse excita-

* Corresponding author. Los Alamos National Laboratory, MST-8, MS E546, Los Alamos, NM 87545, USA. Tel.: +1-505 667 4274; fax: +1-505 665 5849; e-mail: cooke@lanl.gov.

[1] Present address: Department of Physics, University of Memphis, Memphis, TN 38152, USA.

0022-3115/98/$19.00
PII: S0022-3115(98)00027-0

tion and observed a band spectrum initially centered near 2.1 eV that shifted to 2.3 eV within milliseconds after exposure. Comparable luminescence was found in crystalline SiO_2 (c-SiO_2) near 2.8 eV, which had been previously attributed to excitons self trapped at ruptured Si–O bonds [10–12]. Tanimura et al. [9] concluded that the metastable centers in a-SiO_2 were STEs just as in c-SiO_2; their structure was thought to involve oxygen-ion displacement of about 0.03 nm away from the normal lattice site into an interstitial position, accompanied by rupture of a single Si–O bond. Several researchers have suggested that electronic deexcitation of this defect is characterized by luminescence near 2.7 eV, and is thought to be intrinsic to SiO_2 [13–15]. Formation of the STE requires an activation energy because the configurational coordinate must either overcome or penetrate a potential barrier [12–16].

From luminescence lifetime measurements and ab initio molecular orbital calculations, Tohmon et al. [17] proposed an alternative model to describe the 2.7 eV luminescence in a-SiO_2. They suggest the band is associated with triplet-to-ground state transitions of neutral oxygen vacancy defects (≡Si–Si≡). [For an excellent review of the defects found in SiO_2 see D.L. Griscom [18] and references therein]. To date, this model has not gained widespread acceptance.

Direct evidence for self-trapped holes (STHs) in c-SiO_2 does not currently exist; however, Hayes and Jenkin [19] have identified a defect in germanium-doped α quartz that consists of a hole trapped on an oxygen ion bridging lattice silicon with substitutional Ge which, in the absence of Ge, would indeed comprise a STH. The situation in a-SiO_2 is more complex than in c-SiO_2 because of an intrinsic variation in bond strength. The pairwise equivalence of oxygens in c-SiO_2 is not found in the amorphous material because of the inherent randomness of the glassy state. Utilizing electron spin resonance (ESR), Griscom [20,21] has elucidated the structure of two distinct STH centers in a-SiO_2, X-irradiated at 77 K: STH_1 consists of a hole trapped in the $2p$ orbital of a normal bridging oxygen and is viewed as a small polaron. STH_2 probably comprises a hole rapidly tunneling between degenerate valence-band-edge states on a pair of adjacent oxygens.

In the present paper we present measurements of the temperature dependence and relaxation of RL from a-SiO_2 and describe a phenomenological model that adequately explains the observations. The main RL occurs near 550 nm and is attributed to radiative electron-hole (STE) recombination. Thermally-activated exciton quenching, i.e., enhanced nonradiative electron-hole recombination, is believed to be responsible for the observed decrease in RL intensity of the main band at elevated temperatures. An excellent fit to the experimental data is obtained by assuming a polynomial spread in barrier energy to STE quenching. Relaxation of RL with time is associated with the enhancement of nonradiative recombination.

2. Experimental

Four types of a-SiO_2 specimens were obtained from Fiberguide Industries, [22] and were used in the as-received condition. Optical fibers comprised of either low OH (~1 ppm by weight) or high OH (600–800 ppm by weight) doped silica cores with F-doped silica cladding and Al jackets were cut into 2.5-cm sections and placed side by side on an Al sample holder for RL measurements. Optical absorption measurements were made with a Cary 5E spectrophotometer using the standard cutback method [23] with fiber lengths of 50 and 1 m. Typical diameters of the core/cladding/jacket fibers were 200/220/280 μm. The fibers are commercially referred to as anhydroguide™ (low OH) and superguide™ (high OH), and we adhere to this designation throughout our work. Preform material (Heraeus Suprasil F300), from which anhydroguide™ fibers are usually drawn, was also obtained from Fiberguide Industries. Using a core drill we obtained representative specimens of the silica core only, i.e., without the F-doped cladding. The pillbox-shaped core has 10-mm diameter and 1-mm thickness. An irregular shaped sample of core + cladding was also obtained with dimensions ca. 20-mm diameter and 1-mm thickness.

Typical RL measurements were made by mounting specimens on the Al cold finger of a continuous-flow cryostat and cooling to near 4 K. X-radiation entered the evacuated cryostat through a beryllium window and impinged upon the sample to produce luminescence, which was collected by a bifurcated optical fiber. The X-radiation impinging upon the sample was at an angle of 90° with respect to the collection fiber. Light was transmitted to both a cooled photomultiplier tube (S-20Q response) and to the entrance slit of a 1/4-m monochromator, whose output was detected by a charge-coupled device (CCD) comprising an optical multichannel analyzer (OMA). X-ray excitation at each temperature was limited to 25 s with an exposure rate at the sample position of ~1300 R/s, giving an integrated exposure of ca. 3.25×10^4 R per data point. RL spectra for each temperature of interest were obtained in the spectral region 300–800 nm with OMA integration performed over the final 15 s to avoid a small initial transient. Emission spectra were corrected for the nonlinear response of the spectrophotometer, plotted in energy units, and fitted with Gaussian profiles. Relative intensities of emission peaks were extracted from the fitted data and plotted as a function of temperature. Variations in sample configuration, size, and quality of optical coupling precluded measurement of absolute intensities.

3. Temperature dependence

A representative RL spectrum of a-SiO_2 core material taken at 9 K is shown in Fig. 1. The bold solid line is the

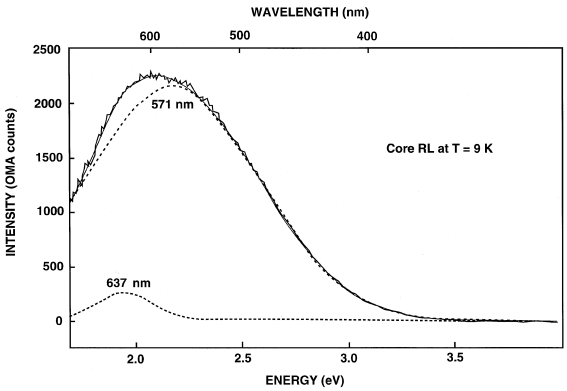

Fig. 1. Radioluminescence emission spectrum of a-SiO_2 core material taken at $T = 9$ K. The bold solid line is the corrected experimental data. Dashed lines are deconvolved Gaussian line shapes, and the smooth solid line is a composite of the two Gaussian bands. Individual peaks are fitted with a linear background term.

corrected data and the dashed lines are the deconvolved individual Gaussian components with peaks at 571 and 637 nm. The composite curve formed by the two Gaussian lineshapes is shown as the smooth solid line, which is in excellent agreement with the experimental data. (Note that the individually fitted peaks are obtained by including a linear background term in the fitting routine; thus the arithmetic sum of individual peak intensities does not equal the composite intensity). This spectrum is typical of the four a-SiO_2 specimens investigated in the present work —main emission in the 550-nm region with secondary emission near 650 nm. Origin of the latter emission remains controversial, although many researchers argue that it is associated with nonbridging oxygen hole centers (NBOHC; ≡Si–O ·) [18]. A second model, however, suggests that the emission is due to interstitial oxygen atoms produced by photolysis of interstitial ozone molecules [24]. Utilizing site-selective laser spectroscopy, it has recently been argued that 650-nm emission (1.9 eV luminescence band) cannot be due to ozonide molecular ions, and must be attributed to NBOHCs [25]. In contrast, there is a general consensus that a-SiO_2 emission in the 500-nm region can be ascribed to STEs [26]. Assuming STEs are responsible for the main (~ 550 nm) RL emission in a-SiO_2, we focus our attention on the temperature dependence of RL emission intensity and ignore the relatively small temperature-dependent variations in peak position and width. Our objective is to combine experimental RL data with model calculations to gain a better understanding of this dominant emission mechanism in a-SiO_2.

Fig. 2 shows the temperature dependence of the 571-nm RL peak intensity taken at 10 degree intervals. The intensity decreases with increasing temperature at a nonexponential rate. For competition between radiative and nonradiative transitions within a luminescence center, the classical theory predicts that the temperature dependent intensity can be described by the expression [27]

$$L(T) = \frac{1}{1 + ae^{-b/T}}. \tag{1}$$

Mattern et al. [26] indeed fitted a 3-eV RL band found in synthetic quartz to this expression and obtained reasonable agreement between data and theory. However, our attempts to use this classical expression to fit the present data were unsuccessful and, consequently, we developed a phenomenological equation that more adequately fitted our experimental results.

We begin the development of this equation by assuming that the decrease in RL intensity with temperature arises from quenching of the radiation from STEs by nonradiative recombination (NRR) of electrons and holes, and proceed to develop an appropriate description of the process represented diagramatically in Fig. 3. The rate of change of STE concentration is

$$\frac{dn}{dt} = \alpha I - \beta n - \gamma n, \tag{2}$$

where the first term on the right αI represents the generation of STEs at radiation intensity I. The second and third terms represent radiative and nonradiative recombination of STEs, respectively. We allow for the possibility that the NRR rate is altered by irradiation of the sample through the simple form

$$\frac{d\gamma}{dt} = \kappa I - \lambda[\gamma - \gamma(T)], \tag{3}$$

where $\gamma(T)$ is the initial value of the NRR rate and κ is the nonradiative enhancement (NRE) parameter. At con-

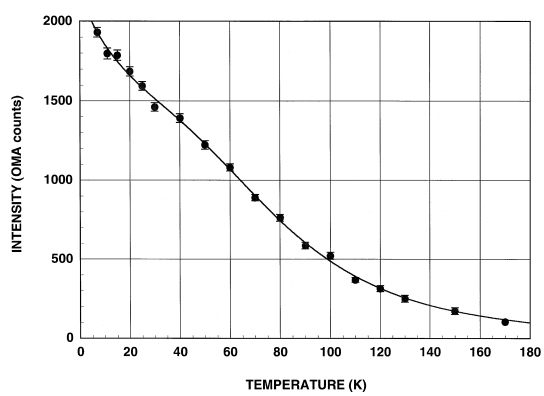

Fig. 2. Temperature dependence of the 571-nm band shown in Fig. 1. Solid circles are experimental data points and the solid line is a fit to Eq. (14) of the text. Fitted parameters are given in the text.

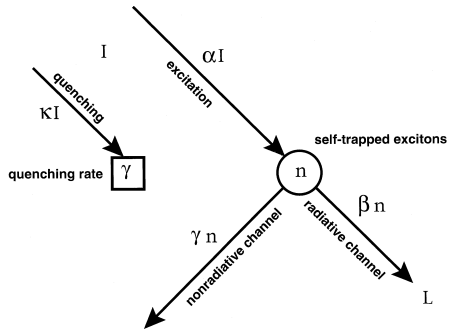

Fig. 3. Model of radiative and nonradiative recombination of self-trapped excitons (STEs). The incident radiation leads to the creation of STEs that decay either through radiative or nonradiative channels. In addition, the incident radiation enhances the branching ratio into the nonradiative channel.

stant radiation intensity, the NRR rate increases from Eq. (3) as

$$\gamma(T,t) = \gamma(T) + \frac{\kappa I}{\lambda}(1 - e^{-\lambda t}). \tag{4}$$

We assume that the exciton relaxation rate from Eq. (2), $\beta + \gamma$, is much greater than the NRE relaxation rate λ. This assumption allows us to take for the instantaneous STE concentration the steady-state value corresponding to the current NRR rate:

$$n(T,t) = \frac{\alpha I}{\beta + \gamma(T,t)}. \tag{5}$$

The luminescence arising from radiative recombination of STEs is then given with $\mu(T,t) \equiv (1/\beta)\gamma(T,t)$ by

$$L(T,t) = \beta n = \frac{\alpha\beta I}{\beta + \gamma(T,t)} = \frac{\alpha I}{1 + \mu(T,t)}. \tag{6}$$

Now we examine various models of temperature-induced decay, which we attribute to STE quenching. The simplest model is a single well-defined barrier to NRR with

$$\mu(T) = \mu e^{-\varepsilon/k_B T}, \tag{7}$$

where μ is the prefactor and ε represents the difference in barrier penetration for nonradiative and radiative recombination. Substituting into Eq. (6) gives for the initial RL:

$$L(T,0) = \frac{\alpha I}{1 + \mu e^{-\varepsilon/k_B T}}. \tag{8}$$

Assuming that α is only very weakly temperature dependent, we write approximately for the initial luminescence

$$L(T) \approx \frac{L(0)}{1 + \mu e^{-\varepsilon/k_B T}}. \tag{9}$$

This expression is equivalent to the classical expression, Eq. (1), previously discussed, but does not yield a good fit to our data.

By assuming an energy spread in the relative barrier penetration we may obtain arbitrary temperature dependence of the luminescence. In this case Eq. (7) can be generalized to

$$\mu(T) = \int_0^\infty \mathrm{d}\varepsilon \mu(\varepsilon) e^{-\varepsilon/k_B T}, \tag{10}$$

with $\mu(T)$ the Laplace transform of $\mu(\varepsilon)$ [28]. We take $\mu(\varepsilon)$ to be a polynomial in ε:

$$\mu(\varepsilon) = \mu_0 + \mu_1\varepsilon + \frac{1}{2}\mu_2\varepsilon^2 + \ldots + \frac{1}{n!}\mu_n\varepsilon^n + \ldots \tag{11}$$

Substituting into Eq. (10) yields

$$\mu(T) = k_B T\left[\mu_0 + \mu_1(k_B T) + \mu_2(k_B T)^2 + \ldots + \mu_n(k_B T)^n + \ldots\right], \tag{12}$$

leading with Eq. (6) to the temperature-dependent RL:

$$L(T) = \frac{L(0)}{1 + \left[\mu_0(k_B T) + \mu_1(k_B T)^2 + \mu_2(k_B T)^3 + \ldots\right]}. \tag{13}$$

Terminating the expansion in T at the cubic term, and simplifying, we successfully fitted all of the RL data to an expression of the form

$$L(T) = \frac{L(0)}{1 + AT + BT^2 + CT^3}. \tag{14}$$

As shown by the solid line in Fig. 2, the RL data for core a-SiO_2 is well fitted by Eq. (14) with the parameters given in Table 1. The fitting routine is based on the standard

Table 1
RL fitted parameters

Figure	$L(0)$, 10^3	A (10^{-2} T^{-1})	B (10^{-4} T^{-2})	C (10^{-6} T^{-3})	ε_{min}/k_B (K)	R^2
(2) Core	2.18	2.08	−3.51	4.92	71.4	0.999
(5) Core/Clad	2.28	1.11	−2.27	3.97	57.2	0.993
(7) Low OH	0.361	1.95	−3.37	4.62	73.0	0.990
(9) High OH	0.565	0.213	−0.583	0.642	90.8	0.886

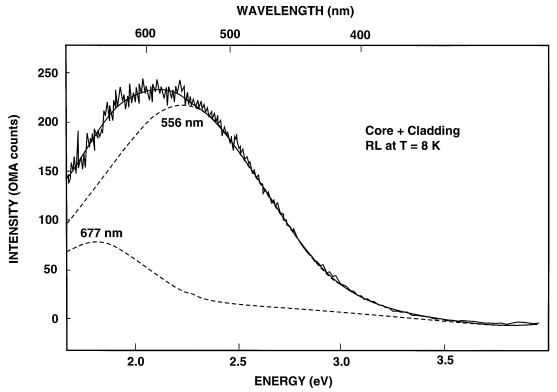

Fig. 4. Radioluminescence emission spectrum of a-SiO_2 core + cladding material taken at $T = 8$ K. The bold solid line is the corrected experimental data. Dashed lines are deconvolved Gaussian line shapes, and the smooth solid line is a composite of the two Gaussian bands.

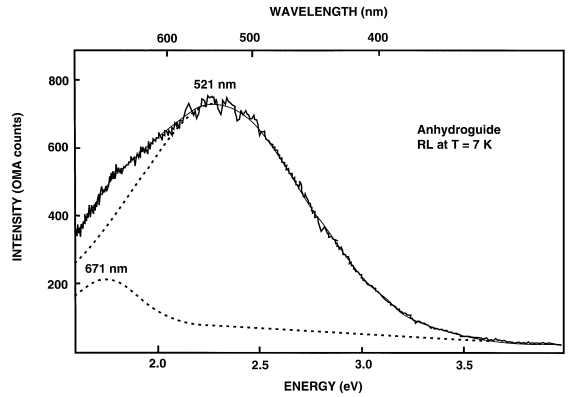

Fig. 6. Radioluminescence emission spectrum of a-SiO_2 anhydroguide™ (low OH) fiber taken at $T = 7$ K. The bold solid line is the corrected experimental data. Dashed lines are deconvolved Gaussian line shapes, and the smooth solid line is a composite of the two Gaussian bands.

linear least-squares method with regression coefficient R^2 [29].

The RL spectrum of the core + cladding specimen taken at $T = 8$ K is shown in Fig. 4, and is similar to that obtained from the core alone. The fitted maxima, shown by the dashed lines, occur at 556 and 677 nm with a ratio of main (556 nm) to secondary (677 nm) intensity of ca. 3. This can be compared to a ratio of ca. 7 for the core sample. The smooth solid line represents the sum of the individual peaks. Fig. 5 depicts the temperature dependence of the main RL peak along with a fit (shown as the solid line) to Eq. (14). The fitted parameters are given in Table 1. Recall that the core and core + cladding samples were taken directly from the preform and are approximately pillbox shaped. We now consider RL results from the two drawn fiber specimens, anhydroguide™ (AG) and superguide™ (SG). Fig. 6 shows the RL of AG taken at $T = 7$ K with Gaussian peaks (dashed lines) at 521 and 671 nm. The approximate ratio of the peak intensities is 3.5, similar to that measured in the core + cladding sample. The temperature dependence of the RL main peak is illustrated in Fig. 7 and is fitted by Eq. (14) with the parameters given in Table 1.

Radioluminescence results from SG taken at $T = 8$ K are shown in Fig. 8. A main peak exists at 596 nm with only a hint of a secondary peak at 660 nm. In fact, this latter peak is sufficiently weak to preclude any meaningful Gaussian fit; the solid line is a Gaussian fit to the main peak only. The RL temperature dependence is illustrated in Fig. 9. A best fit to the experimental data is obtained and shown as the solid line with the parameters given in Table 1.

Note that B and thus μ_1 is negative for all four samples whereas A and C are positive. This condition presumably arises from an initial increase with energy in

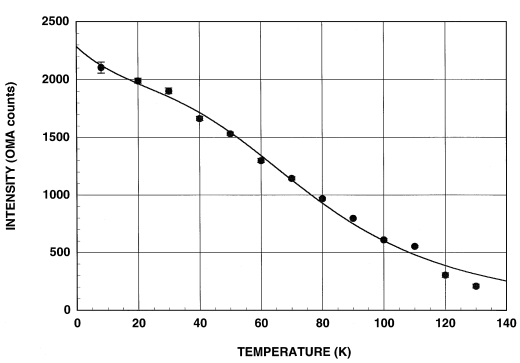

Fig. 5. Temperature dependence of the 556-nm band shown in Fig. 4. Solid circles are experimental data points and the solid line is a fit to Eq. (14) of the text. Fitted parameters are given in the text.

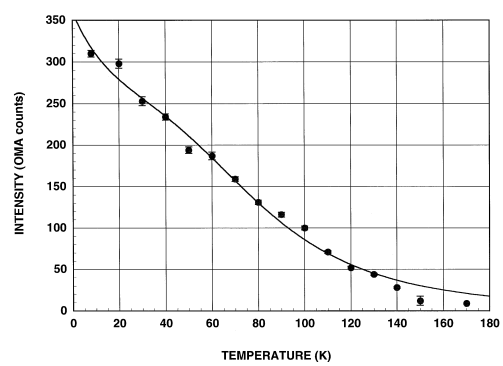

Fig. 7. Temperature dependence of the 521-nm band shown in Fig. 6. Solid circles are experimental data points and the solid line is a fit to Eq. (14) of the text. Fitted parameters are given in the text.

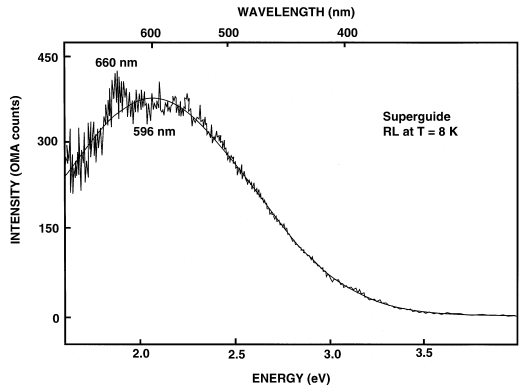

Fig. 8. Radioluminescence emission spectrum of a-SiO_2 superguide™ (high OH) fiber taken at $T = 8$ K. The 660-nm peak was not fitted because of its relatively low intensity. The bold solid line is the corrected experimental data and the smooth solid line is a fitted Gaussian line shape.

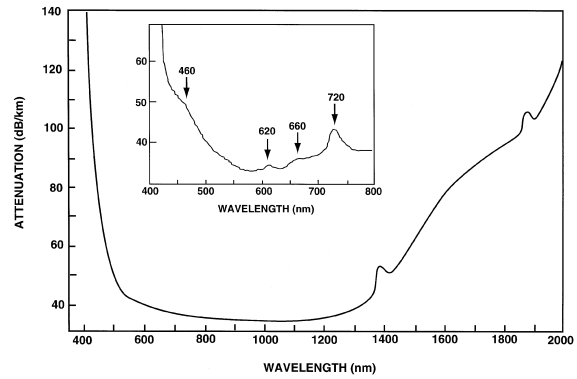

Fig. 10. Optical attenuation of a-SiO_2 anhydroguide™ fiber obtained by the cutback method. The inset shows a separate attenuation measurement obtained with reduced spectral scan rate and enhanced sensitivity over the spectral region 400 to 800 nm.

the probability of radiative recombination and leads to the weak shoulder observed in the RL intensity.

To demonstrate the quality of the optical fibers, we show in Fig. 10 the optical attenuation of a pristine AG fiber. Over a large portion of the visible and near infrared spectral region the attenuation is less than 40 dB/km. This low attenuation necessitated use of the cutback method [23] for determination of the attenuation values. The discernible peaks near 1400 and 1900 nm are attributable to overtone and combination bands of the residual OH impurity [30]. Of course the SG fiber, with its higher OH content (600–800 ppm compared to ~ 1 ppm for AG) exhibited much stronger attenuation at these peak positions. A comparison of optical attenuation in pristine and neutron-irradiated AG and SG fibers has been given by Cooke et al. [31]. The inset of Fig. 10 shows a separate measurement, taken with reduced scan rate and enhanced spectrophotometer sensitivity, of the attenuation of AG fiber with discernible peaks at 460, 620, 660 and 720 nm. These extremely weak absorption bands are either intrinsic or possibly induced by the fiber drawing process [32]. Given the magnitude of pristine absorption, it is reasonable to conclude that the RL emission is associated with radiation-induced rather than existing defects, supporting the model of a STE at a ruptured Si–O bond [9,33].

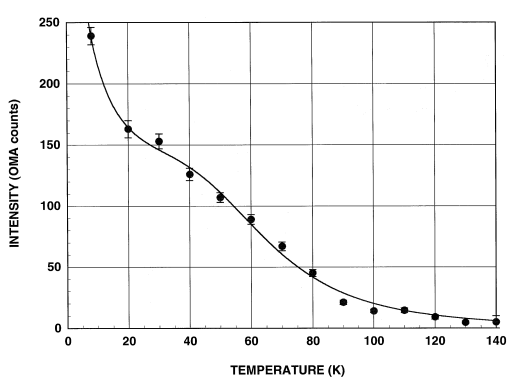

Fig. 9. Temperature dependence of the 596-nm band shown in Fig. 8. Solid circles are experimental data points and the solid line is a fit to Eq. (14) of the text. Fitted parameters are given in the text.

Finally, we mention that the temperature dependence of the secondary RL emission near 650 nm in each of the specimens behaves quite differently from the main emission. For example, with increasing temperature the secondary emission intensity actually increases and reaches a maximum near 100 K. Further temperature increase causes the intensity to gradually decrease, becoming undetectable above ~ 170 K. We have not attempted to model these results, but note that the thermal behavior is consistent with the known radiolytic reaction:

$$\equiv\text{Si–OH} \rightarrow \equiv\text{Si–O}\cdot + \cdot\text{H}^{\circ}, \qquad (15)$$

where both species on the right have been observed by ESR below ca. 130 K [18]. Thus it is not inconsistent to assign the secondary RL peak in our specimens to NBO-HCs.

4. Time dependence

There are two ways to measure the time dependence of RL in the fibers: (1) Record emission spectra data, fit the main peak with a Gaussian line shape, and plot the fitted maximum intensity as a function of time. (2) Use a photomultiplier tube (PMT) to record the total light emitted as a function of time, irrespective of wavelength.

Errors associated with the first method are due primarily to the accuracy of the Gaussian fitting routine, while the latter method does not differentiate between the type of luminescence emanating from the two peaks. For example,

we have previously argued that the main emission is attributable to luminescence arising from radiative recombination of STEs, whereas the secondary peak is thought to be associated with nonbridging oxygen hole centers [18]. The temperature dependence of RL from these two peaks is quite different; whereas the main emission decays smoothly with increasing temperature, the secondary emission exhibits an initial increase in intensity (up to about 100 K) followed by a gradual decrease. Overall, the secondary peak intensity variation with temperature is relatively small compared to that of the main peak. Accordingly, we assume that some variations also will exist in the *time* dependence of RL from these peaks. Of course if the RL is dominated by the main emission then it is appropriate to use the PMT to record the total light emitted and, further, to associate the measured temporal behavior with luminescence from a single type of center. Moreover, application of this latter method avoids any uncertainty of the fitting routine associated with the shift in wavelength maximum as a function of temperature. Because SG fiber RL is dominated by the main peak over the entire temperature range investigated, we chose to measure its temporal dependence by the latter method.

Fig. 11 shows the temporal dependence of RL from SG fiber taken at five fixed temperatures. Plot symbols represent the experimental data and the solid lines are fits to an equation obtained by assuming the RL is attributable to radiative emission from STEs. The rate of decay of STEs is given by Eq. (2). Allowing for the possibility that the nonradiative recombination rate is increased by irradiation leads to Eq. (3). At constant radiation intensity the nonradiative recombination rate increases from Eq. (3) as given by Eq. (4).

Assuming that the STE relaxation rate from Eq. (2) is much greater than the nonradiative recombination rate from Eq. (3), we take for the instantaneous STE concentration the steady-state value corresponding to the current nonradiative recombination rate as given by Eq. (4). The luminescence arising from radiative recombination of STEs is then given by Eq. (5).

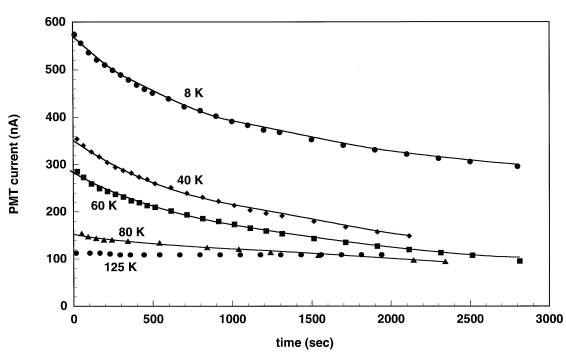

Fig. 11. Temporal dependence of RL from SG fiber at five fixed temperatures. Plot symbols represent the experimental data and the solid lines are fits to Eq. (18) of the text.

Table 2
Relaxation parameters

T (K)	$L(0)$	A	λ, 10^{-4} s^{-1}	$\kappa/\alpha\beta$, 10^{-6}	R^2
8	568	1.25	4.65	1.02	0.999
40	344	0.75	5.26	1.15	0.998
60	284	0.60	4.90	1.04	0.996
80	159	0.219	3.24	0.45	0.989
125	110	< 0.1		< 0.2	

Taking $\mu(T,t) = (1/\beta)\gamma(T,t)$ from Eq. (4) yields the time dependence of the luminescence:

$$L(T,t) = \frac{\alpha I}{1 + \mu(T) + (\kappa I/\beta\lambda)(1 - e^{-\lambda t})}. \quad (16)$$

Alternatively, Eq. (16) may be written in terms of the initial and asymptotic values of the luminescence:

$$L(T,t) = \frac{L(T,0)}{1 + [L(T,0)/L(T,\infty) - 1](1 - e^{-\lambda t})}. \quad (17)$$

Thus, we can quantify the temporal dependence of RL in silica fibers by determining the STE nonradiative recombination rate $\gamma(T,t)$ at any fixed temperature. Accordingly, we fitted our RL data to a function of the form

$$L(t) = \frac{L(0)}{1 + A(1 - e^{-\lambda t})}. \quad (18)$$

The solid lines in Fig. 11 represent a fit of Eq. (18) to the RL as a function of time for fixed temperatures of 8, 40, 60, and 80 K. For $T = 125$ K and above, there is no measurable time decay of RL. Combining Eqs. (16) and (18) gives for the standardized rate of power-induced NRE (cf. Eqs. (2) and (3))

$$\frac{\kappa}{\alpha\beta} = \frac{\lambda A}{L(0)}. \quad (19)$$

A standard linear least-squares fitting routine was used to obtain A and λ in Eq. (18) [29]. The fitted parameters and regression coefficients for each temperature are given in Table 2. The relative NRE rate $\kappa/\alpha\beta$ is seen to drop rapidly above 60 K.

5. Discussion

Radioluminescence data on silica fibers and preforms of the type expected to be used in diagnostic applications show that all are characterized by a main band near 550 nm and a secondary band near 650 nm. These results are similar to those previously reported by Marrone [34] and Miller et al. [35]. The exact spectral peak maxima ex-

tracted from our data vary from sample to sample but the temperature dependence of their RL intensities behave in a similar fashion. In fact, the temperature dependence of the main band RL intensity for each specimen is well described by a model that assumes the emission is reduced by quenching of the radiative STE recombination. We suggest that the main RL emission near 550 nm (2.25 eV) is associated with STEs, consistent with the observations and conclusions of Tanimura et al. [9] and Itoh et al. [33]. Further, we conclude that the secondary RL emission band occurring near 650 nm (1.9 eV) is attributable to NBOHCs. Kalceff and Phillips [36] have recently observed cathodoluminescence emission from synthetic SiO_2 with a maximum near 1.9 eV and concluded that it was consistent with optical absorption of NBOHCs at 1.98 eV, given the predicted Stokes shift of about 0.05 eV [37].

Our results suggest that aside from slight variations in the peak positions of the main and secondary RL spectra, there is essentially no difference in the emission observed from low or high OH content fibers, or from preform material. This implies that RL is associated with major radiation-induced defects in a-SiO_2 rather than subtle ones that are sensitive to fabrication methods or OH content. In other words, it is reasonable to associate RL with commonly occurring defects such as NBOHCs, E′-type centers, and STHs that have been positively identified by ESR methods. The pertinent issue now is the nature of the putative STE in a-SiO_2. That is, what is the trapping site for electrons and holes that comprise the STE?

As previously discussed by Griscom [20], there are two variants of the generic oxygen hole center, STH_1 and STH_2. The former consists of a hole trapped on a normal bridging oxygen ($\equiv Si{-}O\cdot{-}Si\equiv$), and the latter presumably comprises a hole delocalized over two bridging oxygens. The salient feature is that both STHs begin to thermally anneal above $\sim$130 K and completely disappear by $\sim$200 K. These results are consistent with our RL data shown in Figs. 2, 5, 7 and 9, where the RL intensity also becomes undetectable in this approximate temperature range. Now, for charge neutrality there must exist corresponding trapped electrons to compensate for the trapped holes. A diamagnetic electron trap in a-SiO_2 is believed to result from the following [38]:

$$\equiv Si{-}OH + e^- \rightarrow \equiv Si{-}O^- + H^0. \quad (20)$$

Because it is diamagnetic and cannot be detected by ESR, details of this defect are sketchy. Moreover, the reaction given by Eq. (15) apparently competes with a similar well-known radiolytic reaction that produces NBOHCs and atomic hydrogen, the latter thermally decaying above $\sim$130 K:

$$\equiv Si{-}OH \rightarrow \equiv Si{-}O\cdot + \cdot H^0. \quad (21)$$

The branching ratio between these two reactions will likely depend on dose as well as availability of trapping sites for holes. Nevertheless, we see that previously identified defects exist, which, in principle, could form STEs, and that the thermal evolution of these species is consistent with the temperature decay of our RL emission. Consequently, we model the temperature dependent RL in a-SiO_2 as quenching of the STE radiative emission. Assuming a polynomial spread of STE barrier energy, we obtain an excellent fit of the experimental data to the model expression for each of the a-SiO_2 samples, as shown by the solid lines in Figs. 2, 5, 7 and 9.

6. Conclusions

We have measured the RL spectra of a-SiO_2 preform and fiber specimens in the temperature interval 6 to 300 K and wavelength regime 300 to 800 nm. The emission consists of main ($\sim$550 nm maximum) and secondary ($\sim$650 nm maximum) bands that are associated with STEs and NBOHCs, respectively. The temperature dependence of the main emission decays with increasing temperature and is undetectable above 130 to 170 K, the exact value being sample dependent. Thermal evolution of the RL is consistent with the decay of previously identified STHs, NBOHCs, and E′-type centers, suggesting that the putative STE is likely related to the thermal decay of these species. Thermally-activated STE quenching, i.e., enhanced *nonradiative* recombination, is responsible for the observed decrease in RL intensity of the main band at elevated temperatures. By assuming a polynomial spread in barrier energy to STE quenching, we have developed an expression to describe the RL intensity which, when compared with the experimental data, exhibits excellent agreement.

References

[1] E. Udd, Rev. Sci. Instrum. 66 (1995) 4015.
[2] S.F. Paul, J.L. Goldstein, R.D. Durst, R.J. Fonck, Rev. Sci. Instr. 66 (1995) 1252.
[3] P.D. Morgan, Proceedings of the Symposium on Fusion Technology, Rome, Italy, September 14–18, 1992.
[4] A.T. Ramsey, K.W. Hill, Rev. Sci. Instr. 63 (1992) 4735.
[5] H.G. Adler, K.W. Hill, A.T. Ramsey, W. Tighe, Rev. Sci. Instr. 66 (1995) 904.
[6] W. Tighe, P. Morgan, H. Adler, D. Cylinder, D. Griscom, D. Johnson, D. Palladino, A. Ramsey, Rev. Sci. Instr. 66 (1995) 907.
[7] Magnetic Fusion Energy Program Annual Report, 1989, Available from National Technical Information Service, US Department of Commerce, 5285 Port Royal Road, Springfield, VA 22161.
[8] D.L. Griscom, J. Appl. Phys. 77 (1995) 5008.
[9] K. Tanimura, C. Itoh, N. Itoh, J. Phys. C 21 (1988) 1869.
[10] A.L. Shluger, J. Phys. C 21 (1988) L431.
[11] A.J. Fisher, W. Hayes, A.M. Stoneham, Phys. Rev. Lett. 64 (1990) 2667.
[12] A. Shluger, E. Stefanovich, Phys. Rev. B 42 (1990) 9664.

[13] P.J. Alonso, L.E. Halliburton, E.E. Kohnke, R.B. Bossoli, J. Appl. Phys. 54 (1983) 5369.
[14] K. Tanimura, L.E. Halliburton, Phys. Rev. B 34 (1986) 2933.
[15] C. Itoh, K. Tanimura, N. Itoh, M. Itoh, Phys. Rev. B 39 (1989) 11183.
[16] N.F. Mott, A.M. Stoneham, J. Phys. C 10 (1977) 3391.
[17] R. Tohmon, Y. Shimogaichi, H. Mizuno, Y. Ohki, K. Nagasawa, Y. Hama, Phys. Rev. Lett. 62 (1989) 1388.
[18] D.L. Griscom, J. Ceram. Soc. Jpn. 99 (1991) 923.
[19] W. Hayes, T.J.L. Jenkin, J. Phys. C 19 (1986) 6211.
[20] D.L. Griscom, Phys. Rev. B 40 (1989) 4224.
[21] D.L. Griscom, J. Non-Cryst. Solids 149 (1992) 137.
[22] Fiberguide Industries, 1 Bay Street, Stirling, NJ 07980.
[23] D. Marcuse, Principles of Optical Fiber Measurements, Academic Press, New York, 1981.
[24] K. Awazu, H. Kawazoe, J. Appl. Phys. 68 (1990) 3584.
[25] L. Skuja, T. Suzuki, K. Tanimura, Phys. Rev. B 52 (1995) 15208.
[26] P.L. Mattern, K. Lengweiler, P.W. Levy, Radiat. Eff. 26 (1975) 237.
[27] F. Seitz, Trans. Faraday Soc. 35 (1939) 79.
[28] G. Arfken, Mathematical Methods for Physicists, 3rd edn., Academic Press, San Diego, 1985.
[29] P.R. Bevington, Data Reduction and Error Analysis for the Physical Sciences, McGraw-Hill, New York, 1969.
[30] E.J. Friebele, D.L. Griscom, M.J. Marrone, J. Non-Cryst. Solids 71 (1985) 133.
[31] D.W. Cooke, B.L. Bennett, E.H. Farnum, J. Nucl. Mater. 232 (1996) 214.
[32] P. Kaiser, J. Opt. Soc. Am. 64 (1974) 475.
[33] C. Itoh, T. Suzuki, N. Itoh, Phys. Rev. B 41 (1990) 3794.
[34] M.J. Marrone, Appl. Phys. Lett. 38 (1981) 115.
[35] A.J. Miller, R.G. Leisure, V.A. Mashkov, F.L. Galeener, Phys. Rev. B 53 (1996) R8818.
[36] M.A.S. Kalceff, M.R. Phillips, Phys. Rev. B 52 (1995) 3122.
[37] E.P. O'Reilly, J. Robertson, Phys. Rev. B 27 (1983) 3780.
[38] E.H. Nicollian, J.R. Brews, MOS Physics and Technology, Wiley, New York, 1982.